PROPERTIES AND KEPLERIAN ROTATION OF THE HOT CORE IRAS 20126+4104

Jin-Long Xu[1,2,3], Jun-Jie Wang[1,2] and Chang-Chun Ning [2,4]

`xujl@bao.ac.cn`

[1]National Astronomical Observatories, Chinese Academy of Sciences, Beijing 100012, China

[2]NAOC-TU Joint Center for Astrophysics, Lhasa, Tibet, 850000, China

[3]Graduate University of the Chinese Academy of Sciences, Beijing, 100080, China

[4]Tibet University, Lhasa, Tibet, 850000, China

ABSTRACT

We present Submillimeter Array observations of the massive star-forming region IRAS 20126+4104 in the millimeter continuum and in several molecular line transitions. With the SMA data, we have detected nine molecular transitions, including DCN, CH_3OH, H_2CO, and HC_3N molecules, and imaged each molecular line. From the 1.3 mm continuum emission a compact millimeter source is revealed, which is also associated with H_2O, OH, and CH_3OH masers. Using a rotation temperature diagram (RTD), we derive that the rotational temperature and the column density of CH_3OH are 200 K and 3.7×10^{17} cm^{-2}, respectively. The calculated results and analysis further indicate that a hot core coincides with IRAS 20126+4104. The position-velocity diagrams of H_2CO ($3_{0,3}$-$2_{0,2}$) and HC_3N (25-24) clearly present Keplerian rotation. Moreover, H_2CO ($3_{0,3}$-$2_{0,2}$) is found to trace the disk rotation for the first time.

Subject headings: ISM: individual (IRAS 20126+4104) — ISM: kinematics and dynamics — ISM: molecules — stars: formation

1. Introduction

Massive star formation, especially in the earliest phase, is poorly understood, due to the large distances involved (≥ 1 kpc), complex cluster formation environments and shorter evolutionary timescales of massive stars. Hot cores represent the early phase in the process of massive star-formation (Qin et al. 2010). The hot cores are defined as compact ($\leq$ 0.1 pc, n $\geq 10^7$ cm^{-3}), relatively high temperature ($T_k \geq 100$ K) cloud cores (Kurtz et al. 2000). Thus, observation of hot cores with high angular resolution and various molecular lines can provide important information on the early evolutionary phase of massive star formation.

IRAS 20126+4104, at a distance of 1.7 kpc from the Sun (Dame & Thaddeus, 1985; Wilking et al. 1989; Moscadelli et al. 2011), is a massive star-forming region with a bolometric luminosity of $1.3 \times 10^4 L_\odot$. Previous observations of NH$_3$, CH$_3$CN and CS molecular lines toward IRAS 20126+4104 indicated that a Keplerian disk was detected around a $\sim$ 7-24 $M_\odot$ point mass (Zhang et al. 1998; Keto & Zhang 2010; Cesaroni et al. 1999, 2005). Traced in CO, NH$_3$, SiO, HCO$^+$, CH$_3$OH and H$_2$ molecular lines (Shinnaga, et al. 2008; Su et al. 2007; Zhang et al. 1999; Cesaroni et al. 1997, 1999, 2005; Shepherd et al. 2000), a bipolar jet/outflow system was widely investigated toward IRAS 20126+4104. In addition, H$_2$O, OH and CH$_3$OH masers in IRAS 20126+4104 were revealed from observations at centimeter bands (Tofani et al. 1995; Trinidad et al. 2005; Minier et al. 2001; Edris et al. 2005). The CH$_3$OH masers might be associated with a hot core (Minier et al. 2001). From VLA observations toward IRAS 20126+4104, Tofani et al. (1995) did not detect the 1.3 and 3.6 cm continuum emission, but Hofner et al. (1999) detected two elongated structures at the 3.6 cm continuum band. They concluded that the emission was associated with thermal ionized jets and not from a UCHII region. Moreover, IRAS 20126+4104 has the typical colors of UCHII (Wood & Churchell 1989), suggesting that

IRAS 20126+4104 may be a precursor of a UCHɪɪ region (Molinari et al. 1996). Thus, IRAS 20126+4104 provides us with an opportunity to study the early evolution of massive star formation.

We have carried out multiline observations toward the massive star-forming region IRAS 20126+4104 with the Submillimeter Array. Various molecular lines are used to investigate the physical and chemical processes of IRAS 20126+4104. So far, only a few molecular lines exclusively indicate rotational motions (Beuther 2007). In this paper, we find new molecular line (H_2CO) which can trace the Keplerian disk. In Sect. 2, we summarize the observations. In Sect. 3, we give the general results. We discuss core properties and core kinematics in Sect. 4.1 and Sect. 4.2, respectively. In Sect. 5, we summarize our main conclusions.

2.   OBSERVATIONS AND DATA REDUCTION

The data are from SMA archive. Observations toward IRAS 20126+4104 were carried out with the SMA on 2004 August 23, at 218 (lower sideband) and 228 GHz (upper sideband). The typical system temperature was 130 K. The compact configuration with seven antennas was used. The phase center was R.A(J2000.0)= $20^h14^m26^s.00$ and decl.(J2000.0) = $41°13'31''.50$. The spectral resolution is 0.8125 MHz, corresponding to a velocity resolution of 1.1 km s^{-1}. The absolute flux density scales were determined from observations of Uranus, and the bright quasar 3C 279 was used for bandpass calibration. QSO 2015+371 and QSO 2202+422 were observed for the antenna gain corrections. The calibration and imaging were performed in Miriad. The continuum map was made using the line-free channels. The spectral cubes were constructed using the continuum-subtracted spectral channels. Self-calibration was performed to the continuum data. The gain solutions from the continuum were applied to the line data. The synthesized beam size of continuum

and line images with robust weighting was approximately $1''.26 \times 0''.96$ (P.A. $= 89°.0$).

3. RESULTS

3.1. Continuum Emission at 1.3 mm

Figure 1 is the 1.3 mm continuum map of IRAS 20126+4104 obtained by combining the lower and upper sideband data. The continuum emission shows a compact source, which is unresolved in the beam at 1.3 mm. By using a two-dimensional Gaussian fit for the continuum emission, we obtained that the total flux density is 0.62 ± 0.03 Jy, the deconvolved source size is $0.8'' \times 0.5''$ (P.A. $= 87.9°$), and the peak position is R.A.(J2000) $= 20^{\mathrm{h}}14^{\mathrm{m}}26.^{\mathrm{s}}040$ (ΔR.A. $= \pm0.04''$), decl.(J2000) $= +41°13'32.''55$ (Δdecl. $= \pm0.03''$) with an intensity of 0.46 ± 0.05 Jy beam^{-1}. The peak position of the 3.3 mm continuum emission is R.A.(J2000) $= 20^{\mathrm{h}}14^{\mathrm{m}}26.^{\mathrm{s}}008$ (ΔR.A. $= \pm0.01''$), decl.(J2000) $= +41°13'32.''73$ (Δdecl. $= \pm0.01''$) (Cesaroni et al. 1997). For the 7 mm continuum emission (Hofner et al. 1999), the peak position is R.A.(J2000) $= 20^{\mathrm{h}}14^{\mathrm{m}}26.^{\mathrm{s}}026$, decl.(J2000) $= +41°13'32.''70$. The three positions coincide within the uncertainties. H_2O, OH and CH_3OH masers in IRAS 20126+4104 have been detected from observations at centimeter wavelengths (Tofani et al. 1995; Trinidad et al. 2005; Minier et al. 2001; Edris et al. 2005). In Figure 1, H_2O masers are shown with the blue filled triangles. The green open squares present OH masers. The filled black circles show CH_3OH masers. Most of the masers are associated with the 1.3 mm continuum emission, but are not located at the peak position of the 1.3 continuum emission.

3.2.   Molecular Line Emission

In the frequency coverage of the 2 GHz band, deuterated hydrogen cyanide (DCN), formaldehyde (H_2CO), cyanoacetylene (HC_3N) and methanol (CH_3OH) emission lines were identified by use of the CDMS and JPL catalog (Müller et al. 2005; Pickett et al. 1998), as done by other authors in the same frequency range toward Orion (Sutton et al. 1985) and Sgr B2 (Qin et al. 2008). The transition, rest frequency and upper level energy (E_u) of each molecular line are presented in Table 1.

Molecular line images can provide valuable information on the spatial distribution of molecules and kinematics, then we imaged the molecular lines of DCN, CH_3OH, H_2CO, and HC_3N. The 1.3 mm continuum emission has been subtracted before computing these maps. Figure 2 presents the integrated intensity maps of each molecular line. " $\times$ " indicates the peak position of the continuum emission. In Figure 2, each line emission is spatially coincident with the continuum emission.

Spectra of molecular emission are present in Figure 3. The spectra were extracted from the peak positions of each integrated intensity map. We have made Gaussian fits to all the spectra. The central line velocity (V_{LSR}), peak intensity (I_p), and full width at half-maximum (ΔV) are summarized in Table 1.

4.   DISCUSSION

4.1.   Core Properties

Our interferometric continuum and multiline observations toward the massive star-forming region IRAS 20126+4104 reveal a compact millimeter source, which is associated with H_2O, OH, and CH_3OH masers. Millimeter continuum emission mainly traces warm

dust heated by the embedded young stellar object. Four transitions of CH_3OH have been detected in IRAS 20126+4104, so we can use a rotation temperature diagram (RTD) to estimate the rotation temperature and the column density. Assuming local thermodynamic equilibrium (LTE), lines being optically thin and gas emission filling the beam, the rotation temperature and the beam-averaged column density can be expressed by (Goldsmith & Langer 1999; Liu et al. 2002; Qin et al. 2010)

$$\ln(\frac{N_u}{g_u}) = \ln(\frac{N_T}{Q_{rot}}) - \frac{E_u}{T_{rot}}, \tag{1}$$

Where N_u is the column density of the upper energy level, g_u is the degeneracy factor in the upper energy level, N_T is the total beam-averaged column density, Q_{rot} is the rotational partition function, E_u is the upper level energy in K, and T_{rot} is the rotation temperature. Figure 4 is the rotation temperature diagram. A linear least-squares fit is performed toward the four transitions of CH_3OH. The RTD can be corrected by multiplying N_u/g_u by the optical depth correction factor $C_\tau = \tau/(1 - e^\tau)$, where τ is the optical depths. According to Qin et el. (2010), we iteratively applied the C_τ correction to the RTD until the solution converged. After the optical depth is corrected, the rotation temperature and the beam-averaged column density are 200 ± 57 K and $(3.7 \pm 1.3) \times 10^{17}$ cm^{-2}, respectively. The rotation temperature of 200 ± 57 K is the same as that estimated in the CH_3OH (2-1) and (5-4) lines (171 K; Cesaroni et al. 2005), and in the CH_3CN lines (201 K; Cesaroni et al. 1997).

In the Orion molecular cloud, the strongest CH_3OH emission is from the compact ridge (Schilke et al. 1997), giving fractional abundances relative to H_2 of 1.2×10^{-7}. We adopt 0.007 pc as the deconvolved size of the CH_3OH emission derived from the integrated intensity maps of CH_3OH, which is smaller than the canonical size of 0.1 pc that is commonly quoted for hot molecular cores (Kurtz et al. 2000). By using the fractional abundance in the Orion molecular cloud, the calculated H_2 density is 4×10^7 cm^{-3}. The

relatively higher gas temperature (200 ± 57 K), H_2 density ($10^7 cm^{-3}$), and smaller size (0.007 pc) indicate a hot core in this region. Following Gibb et al. (2000), we adopt 3×10^{24} cm^{-2} as a typical H_2 column density. We obtain that the fractional abundance of CH_3OH relative to H_2 is 8×10^{-6}. The fractional abundance of CH_3OH is close to that in the Orion hot core (Blake et al. 1987), but higher than that in the Sgr B2 core (Qin et al. 2008).

4.2. Core Kinematics

The different characteristics of molecular lines may be used as tools to trace various physical processes of massive star formation. To understand the kinematic signatures of the rotating disk, we use the H_2CO ($3_{0,3}$-$2_{0,2}$) and HC_3N (25-24) lines to construct a position-velocity diagram cut through the continuum peak position at a position angle of $58°$. In Figure 5, the continuum emission is redshifted to the southwest and blueshifted to the northeast. The position-velocity diagrams of H_2CO ($3_{0,3}$-$2_{0,2}$) and HC_3N (25-24) clearly present Keplerian rotation. The Keplerian rotation traced in the HC_3N (25-24) line is extremely similar to the model disk constructed by Zhang et al. (1998). So far, for many sources only a few molecular lines exclusively indicated rotating motions in massive star formation (Beuther 2007), e.g., CH_3CN, $C^{34}S$, NH_3, $HCOOCH_3$, $C^{17}O$, $H_2^{18}O$, $HN_{13}C$, HC_3N and CH_3OH. Here we find a new molecule (H_2CO $3_{0,3}$-$2_{0,2}$), which can be used to investigate the rotational signatures of a disk.

In Figure 5, a velocity gradient in the NE-SW direction is clearly depicted. The velocities of the two emission peaks are -6.0 and -2.0 km s^{-1} with 0.60″ separation for the H_2CO ($3_{0,3}$-$2_{0,2}$) molecule, and -5.6 and -3.0 km s^{-1} with 0.55″ separation for the HC_3N (25-24) molecule, respectively. Assuming equilibrium between the rotational and

gravitational force at the outer radius of the Keplerian disk:

$$M_{\text{rot}} = \frac{V^2 r}{G} = 2.3 \times 10^2 \, V^2 (\text{km s}^{-1}) r(\text{pc}) \, M_{\odot}, \tag{2}$$

where V is the velocity difference, r is the spatial separation of the emission peaks and G is the gravitational constant. The derived dynamical mass is 18.0 $M_{\odot}$ and 7.1 $M_{\odot}$ in the H_2CO ($3_{0,3}$-$2_{0,2}$) and HC_3N (25-24) molecular lines, respectively. The calculated dynamical mass is smaller than a mass of $\sim 20 \, M_{\odot}$ obtained by Zhang et al (1998) in the NH_3 molecular lines.

5. SUMMARY

We have observed the massive star-forming region IRAS 20126+4104 in the millimeter continuum and in several molecular line transitions. The 1.3 mm continuum emission reveals a compact millimeter source which is associated with H_2O, OH, and CH_3OH masers. From the SMA data, nine molecular transitions, including DCN, CH_3OH, H_2CO, and HC_3N molecules are detected. The rotational temperature and the column density of CH_3OH emission are 200 K and 3.7×10^{17} cm^{-2}, respectively. The calculated results and analysis further indicate that a hot core coincides with IRAS 20126+4104. A Keplerian rotational disk in the IRAS 20126+4104 hot core is verified in the H_2CO ($3_{0,3}$-$2_{0,2}$) and HC_3N (25-24) lines. H_2CO ($3_{0,3}$-$2_{0,2}$) is found to trace the disk rotation for the first time. The dynamical mass of the Keplerian rotational disk is 18.0 $M_{\odot}$ and 7.1 $M_{\odot}$, determined in the H_2CO ($3_{0,3}$-$2_{0,2}$) and HC_3N (25-24) molecular lines, respectively.

REFERENCES

Beuther, H. 2007, in IAU Symp. 237, Triggered Star Formation in a Turbulent Interstellar Medium, ed. B. G. Elmegreen & J. Palouš (Cambridge: Cambridge Univ. Press), 148

Blake, G. A., Sutton, E. C., Masson, C. R., & Phillips, T. G. 1987, ApJ, 315, 621

Cesaroni R., Felli M., Walmsley C. M., Olmi L. 1997, A&A, 325, 725

Cesaroni R., Felli M., Jenness T., Neri R., Olmi L., Robberto M., Testi L., Walmsley C. M. 1999, A&A, 345, 949

Cesaroni R., Neri R., Olmi L., Testi L., Walmsley C. M., Hofner P. 2005, A&A, 434, 1039

Dame, T. M., & Thaddeus, P. 1985, ApJ, 297, 751

Edris, K. A., Fuller, G. A., Cohen, R. J., & Etoka, S. 2005, A&A, 434, 213

Gibb, E., Nummelin, A., Irvine, W. M., Whittet, D. C. B., & Bergman, P. 2000, ApJ, 545, 309

Goldsmith, P. F., & Langer, W. D. 1999, ApJ, 517, 209

Hofner, P., Cesaroni, R., Rodríguez, L. F., & Martí, J. 1999, A&A, 345, L43

Keto, E., & Zhang, Q. 2010, MNRAS, 406, 102

Kurtz, S., et al. 2000, in Protostars and Planets IV, ed. V. Mannings, A. Boss, & S. Russell (Tucson: Univ. Arizona Press), 299

Liu, S.-Y., Girart, J. M., Remijan, A., & Snyder, L. E. 2002, ApJ, 576, 255

Minier, V., Conway, J. E, & Booth, R. S. 2001, ApJ, 369, 278

Molinari, S., Brand, J., Cesaroni, R., & Palla, F. 1996, A&A, 308, 573

Moscadelli, L., Cesaroni, R., Rioja, M. J., Dodson, R., & Reid, M. J. 2011, A&A, 526, 66

Müller, H. S. P., Schlöder, F., Stutzki, J., & Winnewisser, G. 2005, J. Mol. Struct., 742, 215

Pickett, H. M., Poynter, R. L., Cohen, E. A., Delitsky, M. L., Pearson, J. C., & Müller, H. S. P. 1998, J. Quant. Spectrosc. Radiat. Transfer, 60, 883

Qin, S.-L., Zhao, J.-H., Moran, J. M., et al. 2008, ApJ, 677, 353

Qin, S.-L., Wu, Y. F., Huang, M. H., Zhao, G., Li, D., Wang, J.-J., Chen, S. 2010, ApJ, 711, 399

Schilke, P., Groesbeck, T. D., Blake, G. A., & Phillips, T. G. 1997, ApJS, 108, 301

Shepherd, D. S., Yu, K. C., Bally, J., & Testi, L. 2000, ApJ, 535, 833

Shinnaga, H., Phillips, T. G., Furuya, R. S., et al. 2008, ApJ, 682, 1103

Su, Y.-N., Liu, S. Y., Chen, H. R., et al. 2007, ApJ, 671, 571

Sutton, E. C., Blake, G. A., Masson, C. R., Phillips, T. G., 1985, ApJS, 58, 341

Trinidad, M. A., Curiel, S., Migenes, V., et al. 2005, ApJ, 130, 2206

Tofani, G., Felli, M., Taylor, G. B., & Huang, T. R. 1995, A&AS, 112, 299

Wilking, B. A., Blackwell, J. H., Mundy, L. G., Howe, J. E. 1989, ApJ, 345, 257

Wood, D. O. S., & Churchwell, E. 1989, ApJ, 340, 265

Zhang, Q., Hunter, T. R., & Sridharan, T. K. 1998, ApJ, 505, L151

Zhang, Q., Hunter, T. R., Sridharan, T. K., & Cesaroni, R. 1999, ApJ, 527, L117

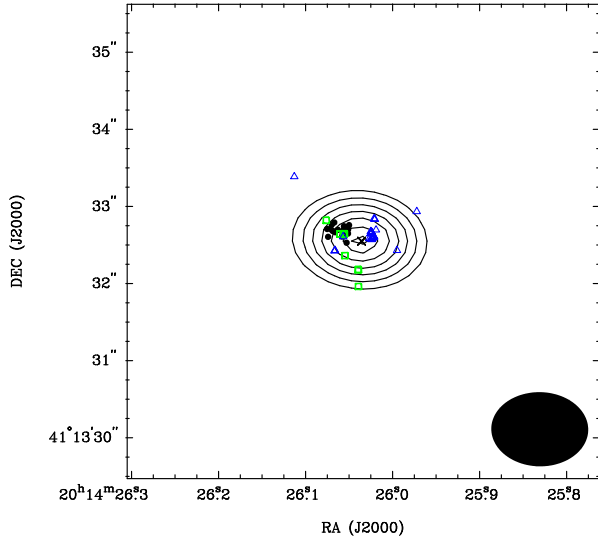Fig. 1.— Continuum map toward IRAS 20126+4104 at 1.3mm obtained by combining the data from both sidebands (218 and 228 GHz). The contours are at -3, 3, 4, 5, 6, 7, 8, and 9 σ. The rms noise level is 0.05 Jy beam^{-1}(1σ). The synthesized beam is $1.3'' \times 0.8''$, P.A.= 88.9° (*lower right corner*). " $\times$ " indicates the peak position of the continuum from the Gaussian fit. H_2O masers are shown with blue filled triangles. The green open squares present OH masers. The filled black circles show CH_3OH masers.
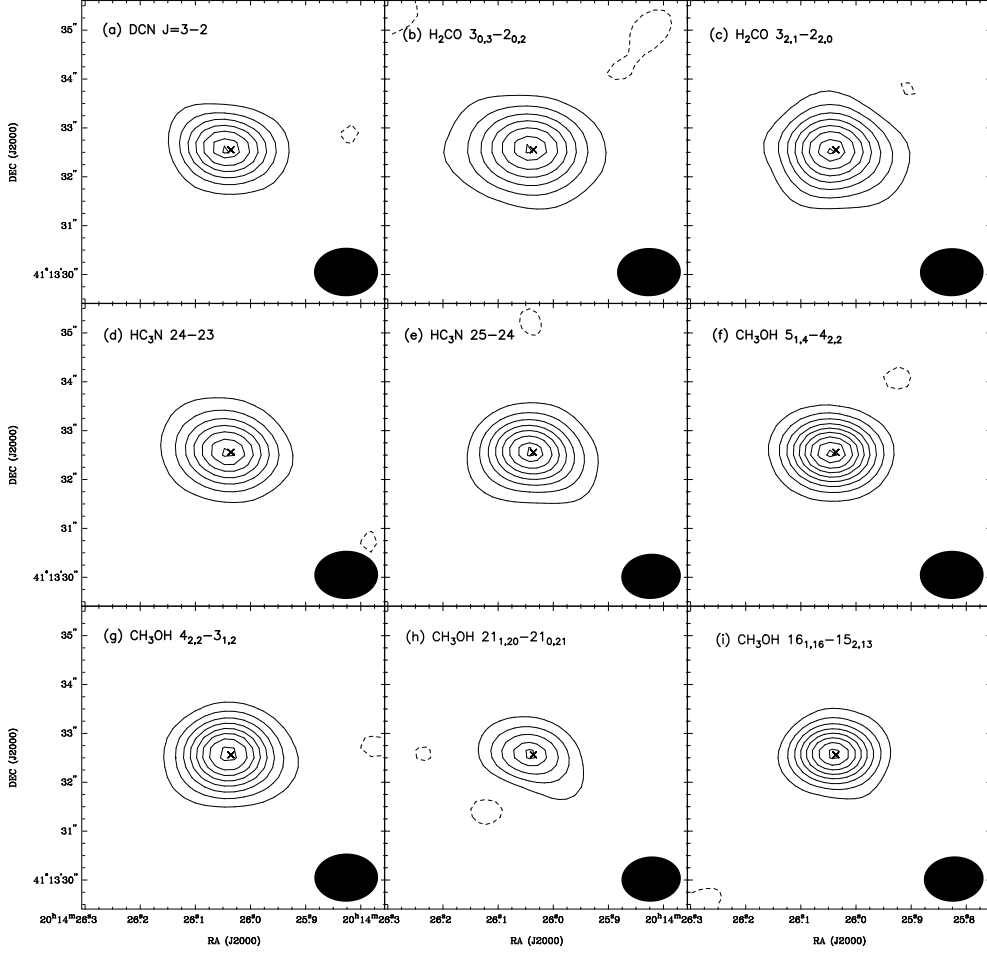
Fig. 2.— (a) The DCN 3-2 integrated intensity map. The contour levels are at -2.2, 2.2, 4.4, 6.6, 8.8, 11.0, 13.2 and 14.3 Jy beam^{-1} km s^{-1}. (b) The H_2CO $3_{0,3}$-$2_{0,2}$ integrated intensity map. The contour levels are at -1.0, 2.5, 5.0, 7.5, 9.0, 12.5, 15.0 and 16.2 Jy beam^{-1} km s^{-1}. (c) The H_2CO $3_{2,1}$-$2_{2,0}$ integrated intensity map. The contour levels are at -1.5, 2.4, 4.8, 7.2, 9.6, 12.0, 14.4, 16.8 and 18.1 Jy beam^{-1} km s^{-1}. (d) The HC_3N 24-23 integrated intensity map. The contour levels are at -1.5, 2.3, 4.5, 6.7, 8.9, 11.1, 13.3 and 15.1 Jy beam^{-1} km s^{-1}. (e) The HC_3N 25-24 integrated intensity map. The contour levels are at -1.6, 2.1, 4.2, 6.3, 8.4, 10.5, 12.6, 14.7 and 15.9 Jy beam^{-1} km s^{-1}. (f) The CH_3OH $5_{1,4}$-$4_{2,2}$ integrated intensity map. The contour levels are at -1.1, 2.2, 4.4, 6.6, 8.8, 11.0, 13.2, 15.4, 17.6, and 19.3 Jy beam^{-1} km s^{-1}. (g) The CH_3OH $5_{1,4}$-$4_{2,2}$ integrated intensity map. The contour levels are at -2.1, 2.8, 5.6, 8.4, 11.2, 14.0, 16.8, 19.6 and 22.8 Jy beam^{-1} km s^{-1}. (h) The CH_3OH $21_{1,20}$-$21_{0,21}$ integrated intensity map. The contour levels are at -1.4, 1.8, 3.6, 5.4, 7.2, and 8.2 Jy beam^{-1} km s^{-1}. (i) The CH_3OH $16_{1,16}$-$15_{2,13}$ integrated intensity map. The contour levels are at -1.5, 2.0, 4.1, 6.1, 8.2, 10.2, 12.2, 14.3 and 16.1 Jy beam^{-1} km s^{-1}. "×"

Table 1: Observed Parameters of Each Line

| Molecule	Transition	Rest Frequency	E_u	V_{LSR}	I_p	ΔV	Channel rms
		(GHz)	(K)	(km s^{-1})	(Jy beam^{-1})	(km s^{-1})	(Jy beam^{-1})
DCN	$3-2$	217.239	20.9	-3.4(0.2)	1.65(0.08)	8.0(0.4)	0.2
H_2CO	$3_{0,3}$-$2_{0,2}$	218.222	21.0	-3.8(0.3)	2.38(0.19)	8.6(0.8)	0.3
	$3_{2,1}$-$2_{2,0}$	218.760	68.1	-5.1(0.3)	2.09(0.13)	7.5(0.6)	0.2
HC_3N	24-23	218.325	131.0	-4.1(0.2)	1.78(0.11)	7.8(0.6)	0.2
	25-24	227.419	141.9	-4.6(0.1)	2.53(0.09)	6.7(0.3)	0.2
CH_3OH	$5_{1,4}$-$4_{2,2}$	216.946	55.9	-3.8(0.2)	2.02(0.12)	8.2(0.5)	0.2
	$4_{2,2}$-$3_{1,2}$	218.440	45.5	-4.1(0.1)	3.01(0.17)	7.3(0.5)	0.2
	$21_{1,20}$-$21_{0,21}$	227.095	557.1	-3.7(0.4)	0.87(0.06)	9.3(0.9)	0.1
	$16_{1,16}$-$15_{2,13}$	227.815	327.2	-4.0(0.2)	1.62(0.07)	8.2(0.4)	0.1
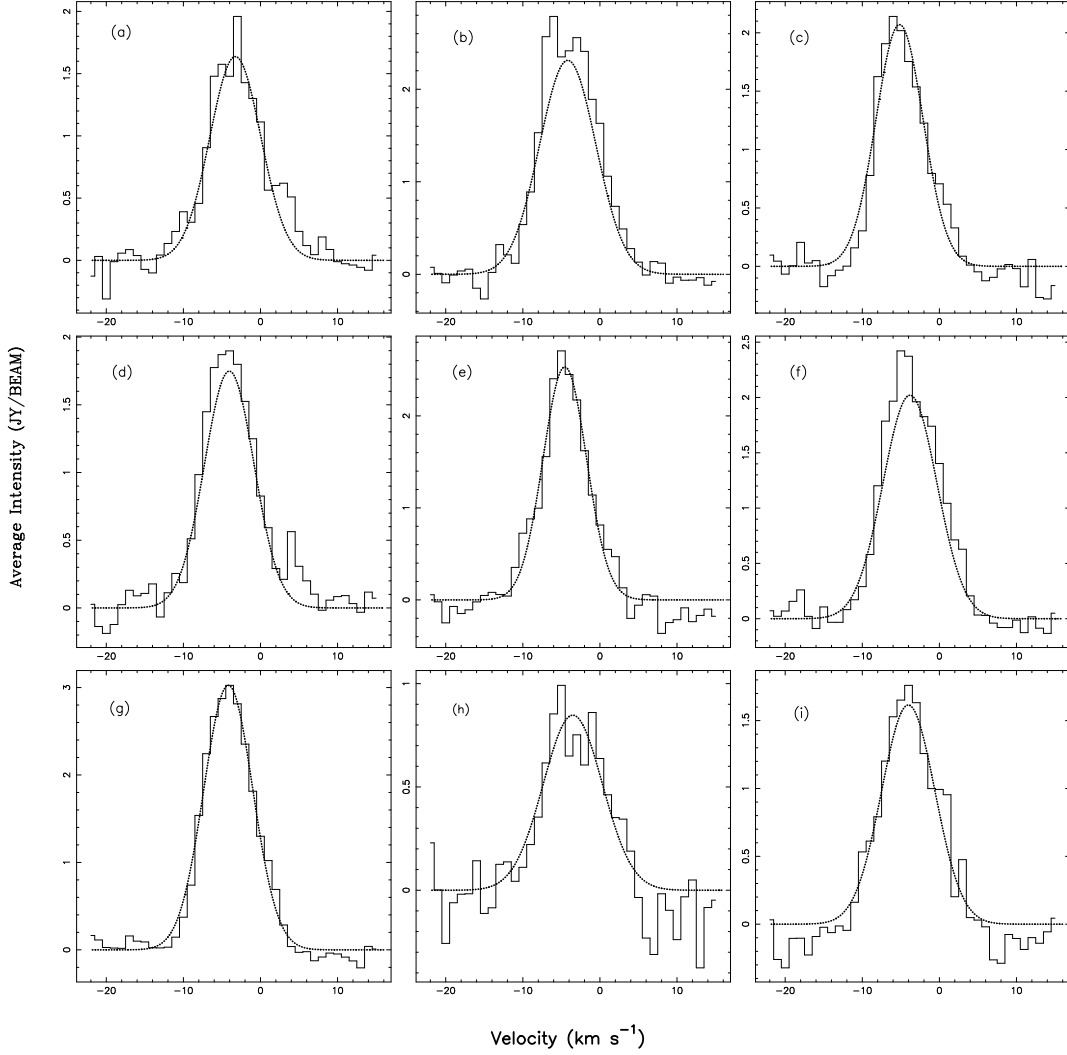
Fig. 3.— Molecular spectra at the peak position of different molecular core. The solid and dashed curves are the observed spectra and the Gaussian fitting to the spectra, respectively. (a) DCN 3-2. (b) H_2CO $3_{0,3}$-$2_{0,2}$. (c) H_2CO $3_{2,1}$-$2_{2,0}$. (d) HC_3N 24-23. (e) HC_3N 25-24. (f) CH_3OH $5_{1,4}$-$4_{2,2}$. (g) CH_3OH $4_{2,2}$-$3_{1,2}$. (h) CH_3OH $21_{1,20}$-$21_{0,21}$. (i) CH_3OH $16_{1,16}$-$15_{2,13}$.
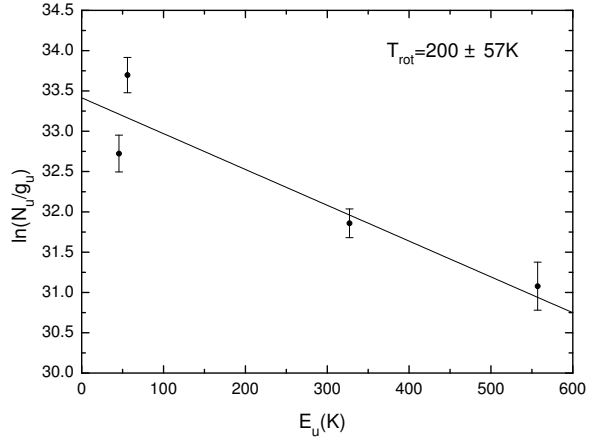
Fig. 4.— Population temperature diagram of the observed CH_3OH transitions. The vertical bars mark the $\ln(N_u/g_u)$ errors from the integrated intensities. The linear least-squares fit (solid line) gives a rotation temperature of 200 ± 57 K.

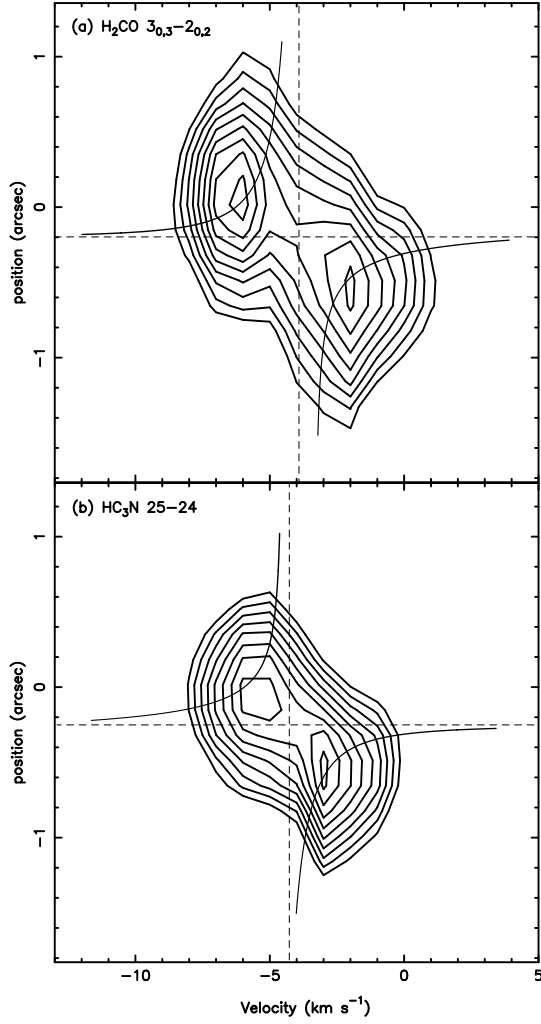Fig. 5.— (a) The position-velocity plot of the H_2CO $3_{0,3}$-$2_{0,2}$ emission at a position angle of $58°$ along the major axis of the disk (Zhang et al. 1999). The contour levels in observed data are plotted at every 2σ. $1\sigma = 0.6$ Jy. Position offsets is $(0.6'', 1.0'')$. (b) The position-velocity plot of the HC_3N 24-23 emission at a position angle of $58°$ along the major axis of the disk. The contour levels in observed data are plotted at every 2σ. $1\sigma = 0.5$ Jy. Position offsets is $(0.6'', 1.2'')$. The horizontal dashed line marks the center of the disk, and the vertical dashed line marks the cloud systemic velocity. The full lines show Keplerian rotation curve.